Paper Type: Original Article

Microseismic Monitoring System for the Management of Seismic Hazard and Rock Bursting and Distribution of Crack

Emad Toghroli[1],* , **Meldi Suhatril[1], Fatemeh Moeini[1], Salman Maleki[1]**

[1] Department of Civil Engineering, Faculty of Engineering, Universiti Malaya, 50603, Kuala Lumpur, Malaysia.
toghroli@calut.au; meldi@um.edu.my; fmoeini@yahoo.com; salmanmakeli1@outlook.com

Abstract

Rockburst is one of the most significant risks that threaten the safety of underground and surface stability and mine operators. Few methods have been generated to evaluate rockburst potential in underground hard rock mines depending on Energy Release Rate (ERR), energy balance, and critical energy and strain Energy Storage Rate (ESR). In this research, a Peak Strength Strain (PSS) of ESR is suggested to estimate and categorize the tendency of rock materials to burst into granite. The energy storage rate index is the elastic Strain Energy Density (SED) rate to the dissipated SED correlated to the peak Compressive Strength (CS) on granite under four orders of magnitude loading ratio. Accordingly, a triaxial unloading limited pressure test was conducted to provide the linear elastic ESR characteristics. Through the use of the Q system, an empirical analysis was performed to check the ratio of σ_1/σ_c to estimate the rockburst. Thus, a twenty-day delay in strain monitoring further changed the PS energy. The findings indicated that the PS energy is roughly 1.3–1.4 times greater than the linear elastic Strain Energy (SE) under the same limited pressure. The deep granite's modified maximum SE value was substantially raised when the time-delay strain effect was considered. The peak strength energy values were raised from 1.0×10^4 J/m³ to 1.8×10^4 J/m³, respectively. Also, the intensity and tendency of rockburst were compared while considering the benefits of the SE index model of rockburst. The primary stress point under various limited pressures was estimated, and the linear elastic SE of deep granite was computed. The test findings show that the linear elastic SED value exhibits a linear growth rule when limited pressure increases. Besides, due to the limited pressure of 40 MPa, the linear elastic SED value of granite is near to $1.3\ e^5$ J/m³. The rock burst grades provided a clear incline ratio after considering the time delay of SE and PS energy. The SED is raised by $4.4\ e^4$ J/m³, under the 40MPa limited pressure. A proper SE technique could bring precise data support for rockburst analysis.

Keywords: Energy storage rate, Energy waste, Distribution of rockburst, Triaxial compressive test.

1 | Introduction

In underground excavation, rockburst is a significant instability problem. In recent decades, enormous endeavours have been made to comprehend and contain the mechanisms underlying rock bursts through suitable rock support structures [1]–[13]. A rockburst is a dramatic displacement or ejection of rock. It makes sense to utilize flexible support structures to restrain rock movement. As a result, in the mines of South Africa in the 1950s and 1960s, split-set friction bolts were first employed to counteract the potential of rockbursts. Split-set bolts are kept in place by creating friction between the borehole wall and the bolt tube. Its inadequate load-bearing capability prevents it from effectively controlling the displacement of rocks. Moreover, all have tried dealing with dynamic stresses using stiff support structures like concrete pillars and enclosed rebar bolts. Yet, the outcomes lacked merit. The cone bolt, a first-yield rockbolt for controlling rockbursts, was created in South Africa in the 1990s [14]. The cementitious grout used to fill the borehole encased the original cone bolt. Later, in Canada, it was altered for use with resin grout [15]. Later, numerous further varieties of energy-absorbing rock bolts were developed [16]–[21]. Surface-holding devices must also be used to yield rockbolts for effective rockburst control. To ensure that all of the components in a support system are correctly connected and jointly create resistance to the ejection of rocks in a rockburst, it is necessary for both the external and internal support devices to be firmly coupled and compatible in deformation. Deep engineering is prone to various catastrophes, including rockbursts, large-scale collapses, slabbing, and massive deformation [22]–[24]. Many theories explain how these disasters happen, including in situ stress [25], [26], rock faults [27], [28], strength theory [29], [30], the energy stored in rocks [31], [32], dynamic disturbance [33]–[36], engineering structures [37], [38], stress monitoring [39], and more [40], [41]. High ground stress is one of the most significant factors contributing to ground pressure disasters. According to numerous studies [30], [42], [43], high-stress locations are where most ground-pressure disasters occur. Gong and Hu et al. discovered through the real triaxial testing of samples with holes that the tangential stress concentration after drilling led to rockburst and spalling in the investigation of the impact of ground stress on ground pressure disasters [44]–[46]. Using numerical simulation, Tao et al. [47] discovered that after excavation, the normal stress release on the free face resulted in rock degradation [48], [49]. Several engineering techniques demonstrate that a quicker excavation speed causes more significant damage to the surrounding rock [50]. This is the usual stress on the excavation surface that can be relieved more quickly as the excavation progresses. Thus, it is important to consider how regular excavation stress releases affect the surrounding rock's surface. As Su et al. discovered, a highly stressed rock mass was excavated, releasing radial tension while concentrating tangential stress [51]. The loading after excavation and the excavation after loading differ somewhat when the starting stress state is considered. When a rock specimen is loaded after excavation, such as during a laboratory test on a rock sample with holes, there is no release of normal stress because there is never any normal tension around the holes. It would be more appropriate to describe deep engineering excavations as a whole when discussing excavations following loads. It's critical to determine the released SE following excavation since this information can be used to predict rockbursts and support energy absorption. Studies on the typical stress release brought on by drilling in deep, prestressed rock are still scarce. In the lab, drilling tests in prestressed rock are challenging. This study suggests a way to determine the SE released during excavation. Laboratory studies and numerical calculations are performed to determine the released SE brought on by drilling in prestressed rock. Further analysis is done on the impact of drilling breadth, height, and lateral pressure on the release of SE. The deep tunnel failure from drilling in prestressed rock is finally simulated numerically. In general, the limited stress has a non-linear relationship with the strength and mass of the rock. As a result, the non-linear Hoek-Brown strength standard is more suitable for rocks and rock masses than the linear Mohr-Coulomb standard. Although extensional fracture happens at the beginning of the loading under unlimited Uniaxial Compression (UC), shear failure typically predominates in the process of breaking the rock. According to the non-linearity in strength, the limited stress affects how the angle of the shear tear plane changes. Others have noted this phenomenon, including Tarasov and Potvin [52]–[54]. However, further research is required to determine the physical process underlying the phenomenon.

Many academics have examined the stress condition of surrounding rock exposed to high temperatures and the thermal impact of rock materials to disclose the effect of temperature on rockburst proneness for hard rock. Real-time high temperature or pre-heating treatment are two frequent heating techniques [32], [55], [56]. In light of the multidimensional stress condition of the deep rock mass at high temperature, space and a free surface are generated following the excavation. Li et al. [57] developed a two-dimensional (2D) geological model using thermal-mechanical coupling and used the "load first, then excavate" technique to simulate rockburst around the high-temperature tunnel. The severity of the surrounding rock's brittle failure and the potential for a more violent rock burst occurrence increased with temperature (20°C–80°C). Yan et al. [58] concluded that high temperatures would increase the severity of rock bursts by numerically analysing the stress distribution properties of tunnels under thermal-mechanical coupling. Some researchers used three-dimensional (3D) compression of rock mass to simulate rockbursts on pre-heated granites with various temperatures and degrees of thermal damage to study the impact of temperature on a rockburst disaster in a deep roadway [40], [59]. Thermal damage was observed to postpone the occurrence of rock bursts with greater intensity. It was discovered by comparing the failure phenomenon of granites at ambient temperature that the rockburst proneness of granites only diminishes at temperatures higher than 500°C [60]. Several studies have replicated the rockburst process at various temperatures; however, most are just qualitative evaluations of the relationship between temperature and rockburst proneness. Hence, if the driving mechanism of rock failure can quantitatively explain the rockburst proneness at various temperatures, this fault can be properly rectified. Rockburst is essentially a dynamic collapse process of rock ascribed to an abrupt release of SE that has built up within the rock [61]–[64]. According to [65]–[68], rock's energy storage and dissipation are closely related to the severity of rock bursts. It is widely accepted that temperature changes will affect rock materials' interior structure and mineral makeup, significantly altering their mechanical features and energy evolution characteristics. Hence, examining the temperature effect is essential to accurately assess the rock burst proneness of pre-heated rocks and the basis for assessing rockburst proneness in high-temperature rock engineering.

The UC test is one of the most popular techniques for determining rockburst proneness. This test evaluates rockburst proneness under an unknown in situ stress state. Based on this, numerous researchers have employed UC tests to evaluate rockburst proneness [69]–[71]. The energy impact index (ACF), SE storage index (WET) [65], peak energy impact index (A'CF), the peak SE storage index (Wetp) [31], [72], and the potential elastic SE [67] are conventional rockburst proneness standards. However, the pre-peak compression process of pre-heated (high-temperature) rocks primarily considers the elastic SE and dissipated energy according to the current evaluation methodologies. The results mostly take the form of a ratio, which, as a relative measure, cannot adequately capture the absolute energy released by the pre-heated rock failure [66]. Few researchers have examined the impact of temperature on rockburst proneness from the energy shift of the entire pre-heated rock failure process. Because of this, the current study aims to concentrate on this viewpoint and thoroughly analyze the energy storage, dissipation, and surplus during the compression of pre-heated granite at various temperatures for a precise and quantitative evaluation of rock burst proneness.

Rock burst is a type of geological catastrophe in deep rock engineering typically brought on by the unexpected, rapid release of elastic SE trapped in rocks [62], [73], [74]. Rock bursts typically happen in brittle, hard rock masses near highly stressed underground apertures [25], [75]–[77], resulting in injuries, property damage, and schedule delays [25], [62], [77]. The subject of rock burst has recently gained popularity in rock engineering and mechanics [64], [78]–[81]. Numerous researchers have concentrated on the tendency of rock materials to burst in the study of rock burst issues. Some discriminant indices have been developed, including the SE storage index [65], decline modulus index [82], rock brittleness index [67], the potential energy of elastic strain [67], and the excess energy index [83]. In the available literature, the index W_{et} has been the one that has been most frequently utilized to evaluate the brittleness, hardness, and rock burst proneness of rocks [67], [80], [84]. At a stress level of 80–90% of the PS of the rock sample, the index W_{et} is determined as the rate of the elastic SED to the dissipated SED, and the appropriate unloading test must be performed. This article replaces SE with SED to facilitate computation [65]. In actuality, the indoor rock burst phenomenon of rock materials

does not appear until the applied force approaches the maximum strength of the rock specimen. As a result, it is important to explore the proportional relationship between the elastic SED and the dissipated SED at the rock sample's maximal strength since it can be used to determine how likely the rock is to burst. The strength of any rock sample cannot be predicted because of the brittleness and variability of natural rock materials [85]. The equivalent ratio of elastic SED to dissipated SED cannot be computed because it is impossible to unload a rock specimen when it is at its strongest. Tunnel surface supports are depicted in *Fig. 1*. This phrase refers to the system of structural components utilized to stabilize the surrounding rock or soil during excavation. In order to protect workers and maintain the structural integrity of the tunnel, it is crucial to prevent collapses and other sorts of instability. Steel ribs or arches, shotcrete or concrete lining, and rock bolts or anchors are a few typical methods of surface support. Depending on the geological conditions, the size and shape of the tunnel, and the intended usage of the tunnel, the precise type and design of surface support will be used.

Fig. 1. Surface supports in tunnel schematic view.
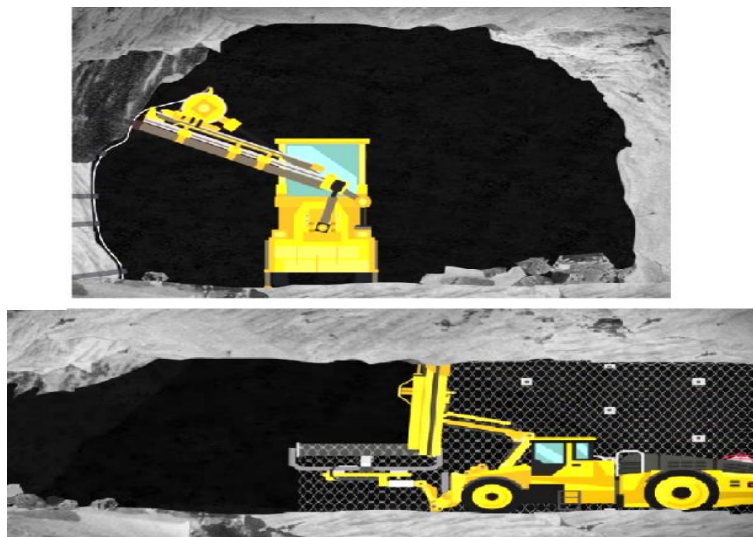
To address the aforementioned issue, the PSS energy storage index W_{et}^p is introduced in this study, which is calculated as the rate of the elastic SED to the dissipated SED at the PS of a rock sample. A series of single-cycle unloading-loading UC experiments were performed for nine rock materials with varying unloading stresses. A method for calculating the elastic SED and the dissipated SED at the PS of a rock sample is suggested. This method is based on the linear relationships between the elastic SED and the total input energy density under various unloading stress levels. W_{et}^p can then be calculated using the results. Furthermore, proposed and addressed is a new categorization criterion for rock burst proneness based on the distribution of W_{et}^p and the actual degree of bursting of nine rock types.

1.1 | Problem of Statement

The problem statement describes the issue of rockburst, which is a significant risk to the safety of underground and surface stability in hard rock mines. The proposed solution uses a PSS of ESR to estimate and categorize the tendency of granite to burst in rock materials. The PSS is determined through a triaxial unloading limited pressure test and a twenty-day time delay in strain monitoring. The problem statement in this research is to develop a method to assess and classify the potential of rockbursts in underground hard rock mines. Rockburst is a significant risk that threatens the safety of mine operators and the stability of underground and surface areas. The research proposes a PSS of ESR to estimate and categorize the tendency of granite to burst off rock materials. The study also aims to compare the intensity and tendency of rockbursts while considering the benefits of the SE index model of rockbursts. The researchers conducted a triaxial unloading limited pressure test to provide the linear elastic ESR characteristics and used the Q system to estimate the rockburst ratio. The research also considered the time-delay strain effect and PS energy values to provide more accurate data for rockburst analysis. The problem statement focuses on developing a method

that can accurately evaluate the potential of rockburst and support rockburst analysis. *Fig. 2* shows the mesh handler. To install a mesh to a tunnel wall, clean it, select the appropriate mesh, cut it to size, apply adhesive to the wall, press the mesh onto the adhesive, allow it to dry, and finish the installation. It's recommended that you consult with a professional contractor for this task.

Fig. 2. Mesh handler instalment on the tunnel walls.

1.2 | Research Questions

I. How does temperature affect pre-heated granite samples' energy storage capacity and rock bursting tendency, as specified by the residual elastic energy index and SCLUC test method?

II. What is the relationship between the peak SED and rock bursting tendency of pre-heated granite samples, as measured by the residual elastic energy index and SCLUC test method, and how can this be used to evaluate the explosive potential of rock in high-geothermal rock engineering?

1.3 | Objective of Study

The SCLUC test method was employed in this study to distinguish between the elastic SE and dissipation energy of pre-heated granite samples and maintain the stress state of the rock under UC. First, an analysis of the failure behaviour and energy evolution of pre-heated granite was conducted using a variety of SCLUC experiments. The residual elastic energy index was then utilized to calculate the peak SE densities and identify the rock-bursting tendency of pre-heated granite samples. The effect of temperature on energy storage capacity, linkages between relevant parameters, and the rock-bursting tendency of pre-heated granite samples were all discussed in the last section. The current work reveals how temperature affects the process of rock burst proneness and provides theoretical underpinnings for determining rockburst proneness in high-geothermal rock engineering. Field findings of rock fracture patterns connected to rock bursts were initially published in the study. Two conceptual models are used to explain the energy transformations and energy sources in the rock burst phenomenon. Following that, the fundamentals of rock support for rock burst control are derived from the perspective of energy release and waste. An approach for providing support is then suggested. The safety factor is considered, along with the need for assistance devices. To illustrate the proportions of energy dissipated in the reinforcing rock bolts and the surface-retaining mesh, full-scale effect tests of two support systems are briefly shown. Lastly, three rock-burst control support systems employed in three nations are introduced. The three support systems were designed using various concepts.

1.4 | Significance of Study

The significance of the study lies in its contribution to improving the safety of underground hard rock mines by providing a method to evaluate and classify the potential for rockburst. Rockburst is a significant risk that threatens the safety of mine operators and the stability of underground and surface areas. Therefore, accurately evaluating the potential for rockburst is critical for preventing and mitigating this risk. The proposed PSS of the ESR method and SE index model provide a more accurate and reliable approach to evaluating the potential of rockburst. The study also considers the time-delay strain effect and PS energy values to provide more accurate data support for rockburst analysis. The findings of this research can be

applied in the mining industry to evaluate and classify the potential for rockburst and support risk management strategies. The proposed method can identify high-risk areas and provide a basis for designing appropriate support structures and mining layouts to prevent and mitigate rock bursts. The study can also contribute to developing guidelines and standards for rockburst assessment in the mining industry. *Fig. 3* shows cracked rock texture.

Fig. 3. Cracked rock texture.

2 | Methodology

2.1 | Materials

In this research, the ratio of σ_1/σ_c was used to estimate the rockburst potential of the deep granite samples. This ratio was determined through an experimental analysis using the Q system. The research also compares the intensity and tendency of rockburst while considering the benefits of the SE index model of rockburst. The findings showed that the PS energy was roughly 1.3-1.4 times greater than the linear elastic SE under the same limited pressure. The deep granite's modified maximum SE value was substantially raised when the time-delay strain effect was considered. The PS energy values were raised from 1.0×10^4 J/m^3 to 1.8×10^4 J/m^3. The mechanical characteristics of granite, a common hard rock, changed noticeably with temperature. Granite was chosen as the experimental material for this study. The granite blocks were gathered. Feldspar (65.5%), quartz (22.6%), and mica (3.4%), which together made up 94.1% of the volume of the chosen granite, were also presented in trace amounts (2.7%). The rock utilized for the brittleness behaviour transition study was granite, a typical brittle rock. A 50 mm × 100 mm cylinder was used to gauge the granite's UC strengths at various temperatures. As explained in the next section, several fundamental mechanical and physical parameters of the natural condition were determined by performing UC tests. Granite samples at 25 °C had an average P-wave velocity of 3665 m/s. The elastic modulus E was 32.22 GPa, the average uniaxial CS was 177.02 MPa, and the porosity was 0.45% on average. In this research, σ_c was selected to represent pre-peak energy evolution because *Table 2* revealed that σ_c and σ_f had the same trend as a rise in temperature.
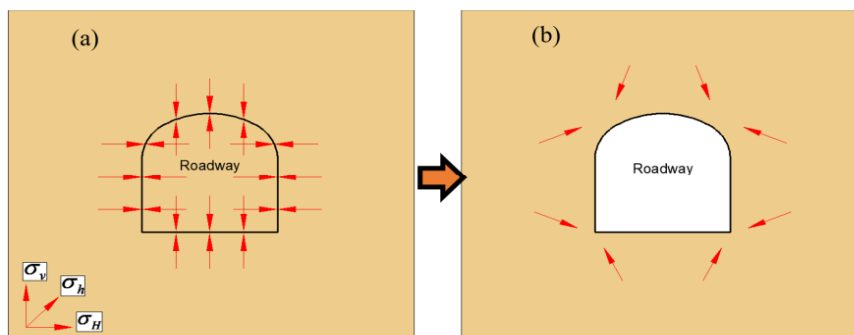

Fig. 4. Excavation-related stress field evolution; a) State of stress before excavation and b) After excavation, there is a release of normal tension and a concentration of tangential stress [86].

2.1.1 | Test process

The methodology used in this research was to determine the rockburst potential of deep granite samples by measuring the ratio of σ_1/σ_c through an experimental analysis using the Q system. The granite samples used in this research were collected from a hard rock mine and were chosen based on their rockburst proneness. The granite samples were mainly composed of quartz, feldspar, and mica, with small amounts of chlorite. The granite samples were tested at various temperatures using a Ø50 mm × 100 mm cylinder for UC tests to measure their UC strength. The granite samples' average P-wave velocity, porosity, elastic modulus, and uniaxial CS were also measured at 25°C. The research also compared the intensity and tendency of rockburst while considering the benefits of the SE index model of rockburst. The findings showed that the PS energy was roughly 1.3-1.4 times greater than the linear elastic SE under the same limited pressure. The deep granite's modified maximum SE value was substantially raised when the time-delay strain effect was considered. The PS energy values were raised from $1.0 \times 10^4 \, J/m^3$ to $1.8 \times 10^4 \, J/m^3$. The test process also included evaluating the trend of the pre-peak energy evolution with the increase in temperature by measuring the CS at different temperatures. A control computer, a loading system, a 2.5-mm displacement extensometer, and a data collection system made up of the INSTRON 1346 test system were used to conduct the testing. The maximal loading range in the quasi-static loading mode could exceed 2,000 kN. The data collection system logged the stress, and the extensometer with a 2.5 mm displacement measured the strain. Single-cyclic loading and unloading UC tests and UC tests were the two different types of testing that were carried out. First, a 120 kN/min UC test was used to determine the UCS (σ_c) of rock material. The next step was to plan and execute a series of single-cycle compression tests with various unloading stress levels (k, the rate of the stress at the unloading point to σ_c; k = 0.1, 0.3, 0.5, 0.7, and 0.9). The rock specimen was loaded until the stress exceeded $k\sigma_c$ at a rate of 120 kN/min and then discharged at the same rate until the stress was zero. Once the rock sample failed, the specimen was reloaded (σ_c^k was the actual PS of a particular rock sample with an unloading stress level k).

I. Material selection: granite was selected as the experimental material due to its common use in rock engineering and temperature-sensitive mechanical properties.

II. Sample preparation: cylindrical samples with a height of 100mm and a diameter of 50mm were prepared according to ISRM recommendations. The samples were tested in natural conditions and at different temperatures.

III. Temperature control: the samples were heated in an oven to the desired temperature and then equilibrated for a specified time to ensure the entire sample reached the target temperature.

IV. Uniaxial compression testing: the samples were tested in UC using a testing machine. The load was applied at a constant rate until the sample failed. The load-displacement curves were recorded, and the peak load and displacement were measured.

V. Data analysis: the peak load and displacement were used to calculate the uniaxial CS of the sample. The elastic modulus (E) was calculated using the initial slope of the load-displacement curve. The P-wave velocity was measured using ultrasonic testing. The porosity was calculated using the sample dimensions and weight.

VI. SCLUC testing: the SCLUC test method separated pre-heated granite samples' elastic SE and dissipation energy. The test involved applying a cyclic load to the sample and measuring the energy dissipation during each cycle.

VII. Q system analysis: the ratio of σ_1/σ_c was determined through an experimental analysis using the Q system to estimate the rockburst potential of the deep granite samples.

VIII. Strain energy index model: the intensity and tendency of rockburst were compared while considering the benefits of the SE index model of rockburst. The modified maximum SE value was calculated by considering the time-delay strain effect.

IX. Results interpretation: the findings were evaluated and used to examine how temperature affected the granite samples' ability to store energy and the correlations between the relevant factors and susceptibility to rock burst.

X. Conclusion: the research findings were summarized, and conclusions were drawn regarding the impact of temperature on the mechanism of rockburst proneness. The results offered theoretical bases for rockburst proneness evaluation in high-geothermal rock engineering.

Table 1 shows the rock mechanical parameters of granite samples at ambient temperature (25°C). These parameters include the uniaxial CS σ_c in MPa, elastic modulus (M) in GPa, Poisson's rate (ν), and are speed in m/s. For the granite specimens in this study, the uniaxial CS ranges from 158.92 MPa to 171.03 MPa, the elastic modulus ranges from 33.22 GPa to 34.1 GPa, the Poisson's rate is approximately 0.24, and the wave velocity ranges from 2541 m/s to 3044 m/s. These parameters are important in determining the rockburst potential of the granite samples.

Table 1. Granite samples' rock mechanical properties at ambient temperature (25°C).

Uniaxial CS, σ_c (MPa)	Elastic Modulus,	Elastic Modulus, M (GPa)	Poisson's Ratio, ν	Wave Velocity (m/s)
171.03	33.22	0.24	0.24	3044

Table 2 shows the results of various tests performed on granite specimens to determine their mechanical properties. The specimens are subjected to different loading methods at different temperatures, including UC and Cyclic Loading-Unloading Uniaxial Compression (CLUUC). The first column indicates the specimen number, and the second column shows the temperature at which the test is performed. The third column indicates the loading method used for the test. The fourth column indicates the UC strength (σ_c) of the specimen in megapascals (MPa), the maximum stress the specimen can withstand under UC. The fifth column shows the failure strength (σ_f) of the specimen in MPa, the stress at which the specimen fails. The sixth column shows the plastic strain (ε_p) of the specimen in units of 10^{-3}, the permanent deformation occurs after it reaches its maximum stress. The seventh column shows the specimen's elastic modulus (E) in gigapascals (GPa), which measures its stiffness. Finally, the eighth column shows the specimen's P-wave velocity (P) in meters per second (m/s), which measures its ability to transmit seismic waves. This table provides a detailed picture of the mechanical properties of the granite specimens tested, which can be used to assess their rockburst potential and other relevant factors for mining and construction projects.

Table 2. Rock main mechanical parameters of granite samples at various loading methods.

Specimen	Heat	Loading Method	σ_c(MPa)	σ_f(MPa)	$\varepsilon_p(10^{-3})$	E(GPa)	P(m/s)
A1	30	UC	171.01	61.02	0.00733	32.43	3454
A2	30	UC	167.32	145.66	0.00755	32.26	3766
A3	30	CLUUC	171.96	145.34	0.00783	33.11	3744
A4	30	CLUUC	158.91	126.11	0.00774	32.14	3823
A1	200	UC	167.34	154.54	0.00835	30.44	2633
A1,2	400	UC	162.76	144.52	0.00825	30.53	2532
A3,4	400	CLUUC	165.84	144.42	0.00843	30.11	2634

*Single-cyclic loading–unloading uniaxial compression.

2.2 | Impact of Excavation Width and Height on Strain Energy Release

The prior analysis found that digging holes in pre-stressed rock led to the release of the SE of the sample. The impact of excavation height on SE release is important when studying rock mechanics and engineering. Excavation height refers to the hole drilled or cut into the rock. As the excavation height increases, the amount of released SE also increases. This is because as the hole height increases, the rock around the hole is subjected to more stress, which releases more SE.

The impact of excavation, in addition to height and width, also plays a role in determining the amount of SE released. As the width of the excavation increases, the rock around the hole is subjected to more stress, which results in the release of more SE. However, the relationship between excavation width and SE release is not as straightforward as between excavation height and SE release. The width of the excavation also affects the distribution of stress around the hole, which can significantly impact the amount of SE that is released. In general, the strain ERR is an important parameter in rock mechanics and rock engineering, as it can provide valuable information on the stability of rock masses and the behaviour of rock structures under stress. The impact of excavation width and height on SE release can be studied using various experimental and numerical methods, such as the photoelastic, finite element, and boundary element methods. It's also important to mention that the excavation height and width are not the only factors affecting the release of the SE. Other factors, such as the properties of the rock, the type of excavation, and the in-situ stress state, can also play a role [86].
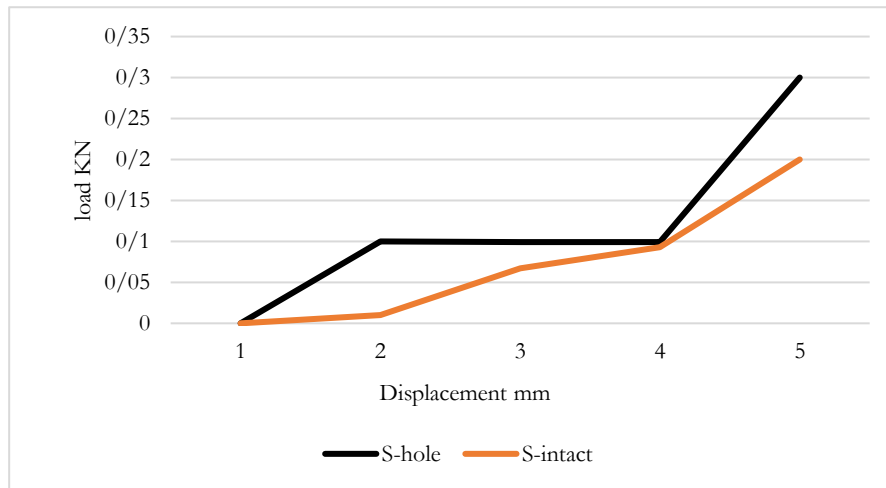

Fig. 5. Curves of samples' loads and displacements.

The loading curve with deformation was chosen to ensure that all samples remained in the elastic stage during testing, and the load versus displacement curves of the two samples are shown in *Fig. 5*. The statement also mentions that the stress-strain curves of the two samples exhibited the characteristics of plastic-elastic deformation. This suggests that the specimens underwent both plastic and elastic deformation during the testing process, which is a common behavior for many materials under mechanical stress.

2.3 | Optimization Theory of the Microseismic Network

One of the variables affecting the accuracy of microseismic data is the spatial array of sensors. An acceptable system placement error is guaranteed when installation horizon, arrangement density, and other factors are considered. Due to the aforementioned issues, optimizing the layout design of the combined system typically involves examining the positioning accuracy error. According to the D-value theory, the error ellipsoid's volume is directly proportional to the size of the determinant of the source parameters' covariance matrix. The technique has been used in several domains [87], [88].

$$T_i = \frac{\sqrt{(x_0-x_i)^2+(x_0-x_i)^2+(x_0-x_i)^2}}{V_p}. \tag{1}$$

When i=1,2,…,n, and n is the number of stations deployed in the mine, V_p stands for the uniform microseismic propagation velocity. Kijko [89], [90] believed that the covariance matrix C_x x of x, as stated in *Eq. (2),* has a role in optimising the sensor station location.

$$C_x = k(A^TA)^{-1}, \tag{2}$$

$$A = \begin{bmatrix} 1 & \dfrac{\partial T_1}{\partial x_0} & \dfrac{\partial T_1}{\partial y_0} & \dfrac{\partial T_1}{\partial z_0} \\ \vdots & \vdots & \vdots & \vdots \\ 1 & \dfrac{\partial T_n}{\partial x_0} & \dfrac{\partial T_n}{\partial y_0} & \dfrac{\partial T_n}{\partial z_0} \end{bmatrix}.$$

A is the estimated partial differential matrix with the associated earthquake arrival time, and k is a constant in *Eq. (2)*. The confidence ellipsoid can be used to visually represent this covariance because its principal axis comprises the length of the covariance matrix's eigenvalues. Choosing the station configuration with the least ellipsoid volume is the optimal design of the D-value. The generation of the covariance eigenvalues or the determinant of C_x determines the ellipsoid's volume. *Eq. (3)* illustrates how det C_x is minimized to meet the D-value optimization standard.

$$obj = m \left(\sum_{i=1}^{ne} M_e(h_i) \lambda x_0(h_i) \lambda y_0(h_i) \lambda z_0(h_i) \lambda t_0(h_i) \right). \tag{3}$$

The number of hypocenter points calculated in the monitoring area, ne, is the variable in the equation. $M_e(h_i)$ is the index for the microseismic event impact factor. The eigenvalues of C_x are $\lambda_{x0}(h_i), \lambda_{y_0}(h_i), \lambda_{z0}(h_i),$ and $\lambda_{t0}(h_i)$.

The unavoidable ground stress changes brought on by mining are accompanied by crack initiation, propagation, and coalescence in the coal rock structure. Energy and materials are exchanged between coal, rocks, and the environment. The total potential energy U for every mechanical system is, according to the principle of minimal potential energy.

$$U = (-W_L + U_E) + U_S. \tag{4}$$

In *Eq. (4)*, U_E stands for the stored SE in a particular system component, W_L for the work that other system components provide to this component, which is comparable to the reduced potential energy in other system components and U_S for the system's dissipative energy. When the coal rock mechanical system is loaded, the external work W_L on the coal rock stress-strain curve can be described as follows:

$$W_L = \int_0^u F du = \int_0^u (F_0 + F_1) du = F_0 u - \frac{1}{2} ku^2. \tag{5}$$

Where k is the dynamic stiffness of the system and F_0 is the system's starting force. Calculations for the variable k include the following:

$$k = \frac{F}{u_0 - u} = -\frac{dF}{du}. \tag{6}$$

Where u is the displacement of the mass of coal and rock and u_0 is the displacement of the loaded system. The area under the curve $f(u) - u$ can be utilized to indicate the strain and dissipation energy of the coal and rock mass. And so

$$U_E + U_S = \int_0^u f(u) du, \tag{7}$$

The system's total potential energy can be stated as follows:

$$U = -F_0 u + \frac{1}{2} ku^2 + \int_0^u f(u) du. \tag{8}$$

The following describes the system equilibrium:

$$\frac{dU}{du} = 0, \text{ namely, } F = f(u). \tag{9}$$

3 | Principles and Requirements of Rockburst Support

3.1 | Monitoring of Mine Seismicity

A rockburst is a severe and sudden underground rock failure caused by releasing stored energy within the rock mass. It can lead to damage to underground structures and loss of life. Rockburst support is a set of techniques and measures to prevent or mitigate rockburst damage. The earliest recorded earthquakes and rock bursts were seen at Creighton Mine in the 1930s, primarily in crown and sill pillars at a depth of 700 meters (2300 feet). Seismicity gradually started to happen in single development headings (also known as strain bursts) at a depth of 1200 m (4000 feet) and in sill accesses following production explosions at a depth of 2000 m (6600 feet). The majority of strain bursts have been linked to geological features. Still, most rock bursts in sill accesses were caused by routine mining activities and typically resulted in sill and crown pillar mining (pillar bursts). The fact that 266 seismic occurrences, or 80% of the total 332 major events, were triggered by fault slippage and just 20% by pillar bursts is noteworthy. If the large-magnitude seismicity at Creighton Mine were known, the rise in large-magnitude events at the other mines suggests a novel pattern that is probably related to the expansion of their mining operations, particularly higher depths and extraction rates. Initiating a systematic approach for managing seismicity and rock bursts, the rock mechanics group at Vale Inco invested in various projects depending on the circumstances. The use of precise numerical modelling to comprehend the behaviour of rock masses is one of these endeavours: 1) testing and putting into use several burst-prone support systems at various mines, 2) putting into practice stope de-stressing in high-stress regions (e.g., the 461 orebodies at Creighton Mine), 3) modify construction techniques and support systems to fit the terrain, such as when working near significant dykes, faults, and shears, 4) increasing the use of microseismic devices and expanding the coverage of seismic sensor arrays inside individual mines and 5) using a 3D Virtual Reality Laboratory (VRL) to comprehend mine seismicity. This leads to the creation of the hazard mapping technique, which is used to pinpoint locations with a high risk of hazard [91].
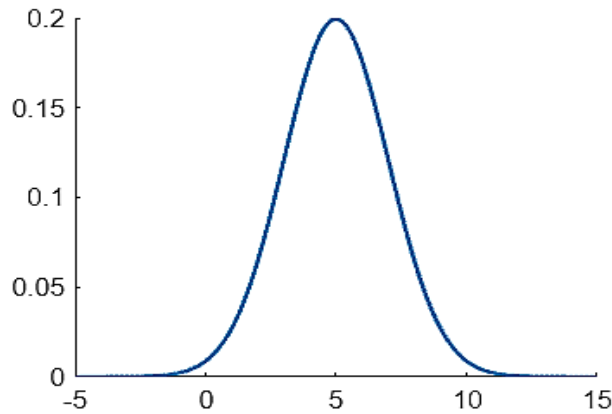
Fig. 6. SE release caused by various widths and heights of excavation holes.

Fig. 6 shows the SE release caused by various widths and heights of excavation holes. When a crack is present in a solid material, the stress distribution near the crack tip becomes highly concentrated, leading to a high potential for fracture or failure. To measure the ability of a material to resist crack propagation, engineers use a parameter called the strain ERR (or simply SE release), defined as the energy required to create a unit area of a new crack surface. When an excavation hole is made in a material, it can cause the stress distribution near the hole to becomes concentrated, much like a crack. The resulting strain ERR is then used to measure the potential for failure near the excavation hole. The strain ERR is calculated using the Stress Intensity Factors (SIF), which are determined by the shape and dimensions of the excavation hole, as well as the properties of the material. In the MATLAB code I provided earlier, the SE release caused by various heights and widths of excavation holes was computed by first defining the input parameters, such as Young's modulus, Poisson's ratio, thickness, height, width, and applied load. Then, the shear modulus, Mode I and Mode II SIFs, total SIF, and SE release are calculated using the relevant equations.
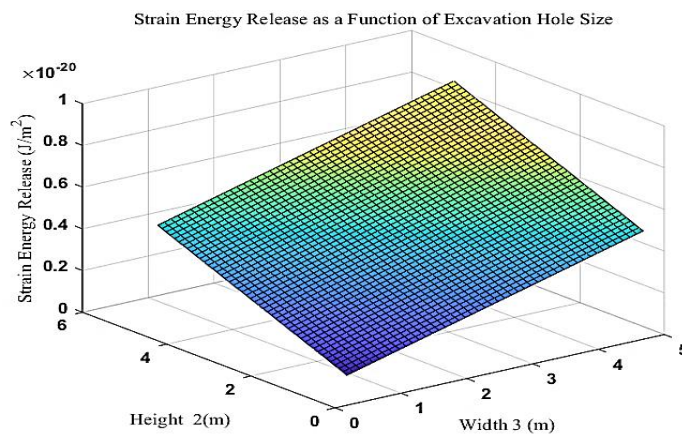

Fig. 7. A 3-D plot of a rectangular excavation hole with a crack length of 1 meter.

Fig. 7 shows a rectangular excavation hole with a crack length of 1 meter. The SE release for an excavation hole with a height of 2.00 m and width of 3.00 m is 0.00 J/m2. The output of this code will be a 3D plot of the SE release as a function of the width and height of the excavation hole. The plot shows the SE release as a function of the width and height of a rectangular excavation hole. The x-axis of the plot indicates the width of the excavation hole in meters. The x-axis range is from 5 to 50 meters, with a step size of 5 meters. The y-axis of the plot represents the height of the excavation hole in meters. The y-axis range is also 5 to 50 meters, with a step size of 5 meters. The z-axis of the plot represents the SE release in joules per square meter (J/m²). The colour of each point on the plot represents the value of the SE release. The colour bar on the right-hand side of the plot shows the correspondence between the colour and the SE release value. The plot shows that the SE release increases as the width and height of the excavation hole increase. A larger excavation hole

creates a larger crack, requiring more propagating energy. The highest SE release values are in the upper-right corner of the plot, where the width and height are 50 meters. Overall, the plot generated by the MATLAB code shows how the dimensions of a rectangular excavation hole can affect the SE release, which is an important factor in understanding the stability and safety of excavations.

3.2 | Management of Seismicity and Rock Bursting

Both strain bursts at rock mass apertures and structurally induced seismicity along structures can result from elevated stresses in mines. The latter may come from high stresses that cause the collapse of Rockbridge in isolated geologically vulnerable zones, fault slides, or fracture propagation. Contrary to popular belief, most geological features, including faults, are not continuous but include entire rockbridges arranged linearly or in an en-echelon arrangement. Major isolated or stepped continuous geological features can cause the complete rock to be destroyed [92]. Rockbursting mechanisms can be better understood with the help of seismic monitoring systems that find, identify, and measure mine seismicity. To increase worker safety and mining production, they help control and mitigate seismic risks. The strategy for mining development and ground support, the use of seismicity for the calibration of numerical models, and the assessment of the restricted access and re-entry protocol are just a few of the topics covered in the discussion of this management that follows.

3.3 | Stress Intensity Factor Hypothesis for Maximum Circumference Tension

Using the minimum SED theory with microseismic monitoring can provide a more comprehensive understanding of the seismic hazard and rockburst potential in a given area. The MSED theory can be used to estimate the SIF of a material's crack, which measures the stress intensity at the crack's tip. This information and data obtained from microseismic monitoring can be used to identify the location and size of potential rock bursts and cracks. Microseismic monitoring systems can detect small seismic events such as rockburst, and by analyzing the data, it is possible to identify the event's location and size as well as the cracks' location and size. The combined use of minimum SED theory and microseismic monitoring can provide valuable information for predicting and mitigating rockburst hazards in underground mining and civil engineering projects. An infinite plate subjected to uniform loading includes a centric mode I and II complex crack. According to linear elastic fracture mechanics, the stress components can be written in the following forms at the crack tip location, based on *Eqs. (10)* and *(11)* [93].

$$\sigma_x = \frac{K_I}{\sqrt{2\pi r}} \cos\frac{\theta}{2}\left(1 - \sin\frac{\theta}{2}\sin\frac{3\theta}{2}\right),$$

$$\sigma_y = \frac{K_I}{\sqrt{2\pi r}} \cos\frac{\theta}{2}\left(1 + \sin\frac{\theta}{2}\sin\frac{3\theta}{2}\right),$$ (10)

$$\tau_{xy}\& = \frac{K_I}{\sqrt{2\pi r}} \cos\frac{\theta}{2}\sin\frac{\theta}{2}\cos\frac{3\theta}{2}.$$

Where K_I and K_{II} are the corresponding SIFs for modes I and II. Adopting the coordinate transformation, the above stresses in a right-angle coordinate system are transformed into circumference stresses in a polar coordinate system, as given by

$$\sigma_x = -\frac{K_{II}}{\sqrt{2\pi r}} \sin\frac{\theta}{2}\left(2 + \cos\frac{\theta}{2}\cos\frac{3\theta}{2}\right),$$

$$\sigma_y = \frac{K_{II}}{\sqrt{2\pi r}} \sin\frac{\theta}{2}\cos\frac{\theta}{2}\cos\frac{3\theta}{2},$$ (11)

$$\tau_{xy}\& = \frac{K_{II}}{\sqrt{2\pi r}} \cos\frac{\theta}{2}\left(1 - \sin\frac{\theta}{2}\sin\frac{3\theta}{2}\right).$$

Where (r, θ) is a local polar coordinate system using the crack tip as an original point.

A circumference tension SIF K_θ is introduced as

$$K_\theta = \lim_{r\to 0}\sqrt{2\pi r}\sigma_\theta = \cos\frac{\theta}{2}\left[\frac{K_I}{2}(1+\cos\theta) - \frac{3K_{II}}{2}\sin\theta\right]. \tag{12}$$

Thus, *Eq. (13)* may be rewritten as

$$\sigma_\theta = \frac{1}{\sqrt{2\pi r}}\cos\frac{\theta}{2}\left[\frac{K_I}{2}(1+\cos\theta) - \frac{3K_{II}}{2}\sin\theta\right]. \tag{13}$$

From hypothesis 1, the opening angle θ can be determined through the attainment of the maximum value condition for *Eq. (12)*, such that

$$\frac{\partial K_\theta}{\partial\theta}\bigg|_{\theta=\theta_0} = 0, \quad \frac{\partial^2 K_\theta}{\partial\theta^2}\bigg|_{\theta=\theta_0} < 0, \tag{14}$$

Then:

$$\left.\begin{array}{l} K_I\sin\theta_0 - K_{II}(3\cos\theta_0 - 1) = 0 \\ K_I\cos\dfrac{\theta_0}{2}(1 - 3\cos\theta_0) + K_{II}\sin\dfrac{\theta_0}{2}(9\cos\theta_0 + 5) < 0 \end{array}\right\}. \tag{15}$$

Combining the two equations from *Eq. (15)*, the opening angle θ_0 can be determined. From hypothesis 2, the fracture criterion is

$$K_{\theta m} = \cos\frac{\theta_0}{2}\left[K_I\cos^2\frac{\theta_0}{2} - \frac{3K_{II}}{2}\sin\theta_0\right] = K_{\theta C}. \tag{16}$$

For an infinite plate subjected to uniform loading with a centric mode I and II complex crack, the displacement fields at the crack tip location are given by

$$u_x = \frac{K_I}{2\mu}\sqrt{\frac{r}{2\pi}}\cos\frac{\theta}{2}\left(\kappa - 1 + 2\sin^2\frac{\theta}{2}\right) + \frac{K_{II}}{2\mu}\sqrt{\frac{r}{2\pi}}\sin\frac{\theta}{2}\left(\kappa + 1 + 2\cos^2\frac{\theta}{2}\right), \tag{17}$$

$$u_y = \frac{K_I}{2\mu}\sqrt{\frac{r}{2\pi}}\sin\frac{\theta}{2}\left(\kappa + 1 - 2\cos^2\frac{\theta}{2}\right) - \frac{K_{II}}{2\mu}\sqrt{\frac{r}{2\pi}}\cos\frac{\theta}{2}\left(\kappa - 1 - 2\sin^2\frac{\theta}{2}\right).$$

Where μ is the shear modulus.

3.4 | Minimum Strain Energy Density Stress Intensity Factor Theory

According to linear elastic fracture mechanics, the stress components at the crack tip location can be found in *Eq. (10)* for the plane problem. For the antiplanet shear mode III crack problem, the SIF K_{III} can be obtained. Thus, the stress field at the crack tip location is given by

$$\tau_{\sqrt{y}} = \frac{K_{1III}}{\sqrt{2\pi r}}\cos\frac{\theta}{2}, \tag{18}$$

$$\tau_{z\pi} = -\frac{K_{1II}}{\sqrt{2\pi r}}\sin\frac{\theta}{2}.$$

Where $K_{III} = S_y\sqrt{\pi a}$, which is dependent on the asymmetric antiplane load S_y and the crack length a. The SED W in an elastic body may be written as

$$W = \frac{1}{2E}\left(\sigma_x^2 + \sigma_y^2 + \sigma_z^2\right) - \frac{\nu}{E}\left(\sigma_x\sigma_y + \sigma_y\sigma_z + \sigma_z\sigma_x\right) + \frac{1}{2\mu}\left(\tau_{xy}^2 + \tau_{FF}^2 + \tau_{zx}^2\right). \tag{19}$$

Substituting *Eqs. (10)* and *(18)* into *Eq. (19)*, an expression for SED at the crack tip location can be obtained.

$$W = \frac{S}{r}. \tag{20}$$

Where S is called the SED factor.

$$S = a_{11}K_1^2 + 2a_{12}K_1K_{II1} + a_{22}K_{II}^2 + a_{33}K_{III}^2. \tag{21}$$

And

$$\left.\begin{aligned} a_{11} &= \frac{1}{16\pi\mu}(1 + \cos\theta)(\kappa - \cos\theta) \\ a_{12} &= \frac{1}{16\pi\mu}\sin\theta(2\cos\theta - \kappa + 1) \\ a_{22} &= \frac{1}{16\pi\mu}[(\kappa + 1)(1 - \cos\theta) + (1 + \cos\theta)(3\cos\theta - 1)] \\ a_{33} &= \frac{1}{4\pi\mu} \end{aligned}\right\},$$ (22)

where

$$K = \begin{cases} \dfrac{3 - v}{1 + v}, & \text{plane stress,} \\ 3 - 4v, & \text{plane strain.} \end{cases}$$ (23)

In minimum SED stress intensity factor theory, the basic hypotheses are

From hypothesis 1, the opening angle θ should satisfy the attainment of the minimum value condition for as follows *Eq. (21)*:

$$\frac{\partial S}{\partial\theta}\bigg|_{\theta=\theta_0} = 0, \quad \frac{\partial^2 S}{\partial\theta^2}\bigg|_{\theta=\theta_0} > 0.$$ (24)

From hypothesis 2, the fracture criterion is

$$S_{min} = S(\theta_0) = S_{minC}.$$ (25)

Where S_{minC} is a critical value of the minimum SED stress intensity factor, which is the material fracture toughness. For the plane strain problem, there are

$$S_{minC} = \frac{1 - 2v}{4\pi\mu}K_{IC}^2.$$ (26)

As a result, *Eq. (25)* has the following form:

$$K_{IC}^2 = \frac{4\pi\mu}{1 - 2v}[a_{11}K_I^2 + 2a_{12}K_I K_{II} + a_{22}K_{II}^2 + a_{33}K_{II}^2].$$ (27)

In a pure mode II crack problem, $K_I = K_{III} = 0$, and obtain from *Eqs. (21)-(24)*:

$$\theta_0 = \arccos\left(\frac{1 - 2v}{3}\right).$$ (28)

Substituting Eq. (23) into *Eq. (21)* and considering *Eq. (25)*, then

$$K_{IIC} = \sqrt{\frac{3(1 - 2v)}{2(1 - v) - v^2}}\,K_{IC}.$$ (29)

If Poisson's ratio $v = 1/3$, then

$$\theta_0 = -83°37', \quad K_{IC} = 0.9K_{IC}.$$ (30)

This result is very close t$K_{IIC} = 0.87K_{IC}$o.

Based on the analysis of linear elastic theory, the concepts of SIF and material fracture toughness have been introduced. An analytical method is given to determine the SIF. The failure criterion and design standard are set for linear elastic fracture mechanics. The stress intensity factor K is a unique quantity that describes the intensity of a crack tip field, which is an important parameter in determining brittle material fracture. For a specific type of fracture, the crack tip field can be fully determined using a parameter K, which can be used to deduce the ERR [93].

3.5 | Discussion

The findings of this research show that the ratio of σ_1/σ_c can be used to estimate the rockburst potential of deep granite samples. The research also found that the PS energy is 1.3-1.4 times greater than the linear elastic SE under the same limited pressure. Additionally, the modified maximum SE value of the deep granite is substantially raised when the time-delay strain effect is considered. The PS energy values were raised from 1.0 $\times$ 104 J/m³ to 1.8 $\times$ 104 J/m³. The research also found that the mechanical properties of granites change significantly with temperature and that the CS of granite increases as the temperature increases. This research also shows that the UC test used in the study is suitable for evaluating the rockburst potential of deep granite samples. Furthermore, the SE index model of rockbursts proved to be a reliable method for comparing the intensity and tendency of rockbursts. On the other hand, the seismic network has picked up 245 earthquakes of varying magnitude, with central distances ranging from 50 - 1400 km. The earthquake signals picked up by the geophones were found to be weak, and the difference in PS wave signals was reflected. In the case of rock bursts, PS waves can be seen depending on the hypocentral interval. In this research, only P-wave onset was utilized to compute rockburst foci, as S-wave onset was not obvious. Microseismic events near the source made differentiating between PS wave signals difficult. Similarly, in the case of normal blasting and deep hole blasting, different P-wave arrivals were recorded because of the various time delays utilized in blasting. The maximum and minimum detectable seismic and micro seismic signal levels were 0.5 to 0.4 millimicrons and 500 to 300 milli-microns, respectively.

4 | Conclusion

As a result of the initial stress field changing due to excavation in pre-stressed rock, normal stress is released onto the free surface, and tangential stress is concentrated. The excavation-related SE release is calculated in this study using a method that involves loading both an intact sample and a sample with holes. The complete specimen experiences an energy transition from loading to excavation to stability (stress balance) that gradually increases SE during loading, decreases SE following excavation, and releases SE after excavation. A fracture zone is produced in the surrounding rock during tunnel excavation in severely strained, fairly hard rock masses. The fracture zone may experience a fault-slip rockburst. For a rockburst to occur, there must be excessive released energy. This energy comes from both the surrounding rock and the ejected rock. The energy absorption capacity of a support system for rockburst control must be greater than the excessive energy to prevent or mitigate rockbursts effectively. This means that the support system must be able to dissipate or absorb the energy released during a rockburst event; otherwise, it will not be able to control the rockburst effectively. This is why it is important to estimate the rockburst potential of deep granite samples and measure the ratio of σ_1/σ_c, as this can provide insight into the amount of energy that could be released during a rockburst event and aid in designing an adequate support system. Furthermore, by measuring the PS energy, linear elastic SE, and modified maximum SE value, one can better understand the energy release mechanism and design an appropriate support system to absorb it. The research also shows that the CS of granite increases as the temperature increases; therefore, considering the temperature effect on the rockburst potential is crucial. Internal reinforcement tendons, such as rock and cable bolts, are more effective at dissipating energy in competent rock mass than surface-retaining devices such as mesh and shotcrete. This is because internal tendons are anchored within the rock mass, providing greater stability and support.

On the other hand, surface-retaining devices are anchored on the surface and provide support by spanning the rock mass, making them less effective in the competent rock mass. However, surface-retaining devices are more effective in soft and weak rock masses as they support the entire surface area, preventing the rock mass from caving in. This is because the rock mass is not strong enough to hold the load of the rockburst, so external support is more effective. Thus, the choice of reinforcement method should be based on the rock mass characteristics and the energy expected to be released during a rockburst event.

Author Contributions

Funding

Data Availability

The data used to support the findings of this study are available from the corresponding author upon request.

Conflict of Interest

The authors declare no conflict of interest regarding the publication of this manuscript.

References

[1] He, M. C., Miao, J. L., & Feng, J. L. (2010). Rock burst process of limestone and its acoustic emission characteristics under true-triaxial unloading conditions. *International journal of rock mechanics and mining sciences*, *47*(2), 286–298. https://doi.org/10.1016/j.ijrmms.2009.09.003

[2] Morrison, R. G. K. (1942). Report on the rockburst situation in Ontario mines. *Trans. canadian institute of mining and metallurgy*, *45*, 225–272.

[3] Kaiser, P. K., Mccreath, D. R., & Tannant, D. D. (1995). *Canadian rockburst research program*. Camiro mining division. https://search.worldcat.org/title/Canadian-rockburst-research-program-1990-1995-:-a-comprehensive-summary-of-five-years-of-collaborative-research-on-rockbursting-in-hardrock-mines/oclc/64385143

[4] Li, C. C. (2017). Principles of rockbolting design. *Journal of rock mechanics and geotechnical engineering*, *9*(3), 396–414. https://doi.org/10.1016/j.jrmge.2017.04.002

[5] Kaiser, P. K. (2018). Chapter 15 - excavation vulnerability and selection of effective rock support to mitigate rockburst damage. In *Rockburst mechanisms, monitoring, warning, and mitigation* (pp. 473–518). Butterworth-Heinemann. https://doi.org/10.1016/B978-0-12-805054-5.00015-9

[6] Salamon, M. D. G. (1983). Rockburst hazard and the fight for its alleviation in south african gold mines. *Rockbursts: prediction and control. symposium* (pp. 11–36). Institution of mining and metallurgy. http://pascal-francis.inist.fr/vibad/index.php?action=getRecordDetail&idt=8453776

[7] Duvall, W. I., & Stephenson, D. E. (1965). Seismic energy available from rockbursts and underground explosions. *Trans. soc. min. eng*, *232*(3), 235–240.

[8] Ortlepp, W. D. (1997). *Rock fracture and rockbursts: an illustrative study* (Vol. 9). South African Institute of Mining and Metallurgy. https://www.google.com/books/edition/Rock_Fracture_and_Rockbursts/tYQQAQAAMAAJ?hl=en

[9] Shan, Z., & Yan, P. (2010). Management of rock bursts during excavation of the deep tunnels in Jinping II Hydropower Station. *Bulletin of engineering geology and the environment*, *69*(3), 353–363. DOI:10.1007/s10064-010-0266-2

[10] Tarasov, B. G., & Stacey, T. R. (2017). Features of the energy balance and fragmentation mechanisms at spontaneous failure of class I and class II rocks. *Rock mechanics and rock engineering*, *50*(10), 2563–2584. DOI:10.1007/s00603-017-1251-x

[11] Feng, X. T., Chen, B. R., Ming, H. J., Wu, S. Y., Xiao, Y. X., Feng, G. L., … & Qiu, S. L. (2012). Evolution law and mechanism of rockbursts in deep tunnels: immediate rockburst. *Chinese journal of rock mechanics and engineering*, *31*(3), 433–444.

[12] Feng, X. T., Xiao, Y. X., Feng, G., Chen, B. R., & Li, S. (2018). Successful examples for mitigating rockbursts in Jinping II tunnels, China. *Rockburst: mechanisms, monitoring, warning and mitigation.* Elsevier, 519–539.

[13] Su, G., Feng, X., Wang, J., Jiang, J., & Hu, L. (2017). Experimental study of remotely triggered rockburst induced by a tunnel axial dynamic disturbance under true-triaxial conditions. *Rock mechanics and rock engineering*, *50*(8), 2207–2226. DOI:10.1007/s00603-017-1218-y

[14] Jager, A. J. (1992). Two new support units for the control of rockburst damage. *International symposium on rock support* (pp. 621–631). A.A. Balkema, Rotterdam. http://pascal-francis.inist.fr/vibad/index.php?action=getRecordDetail&idt=6463792

[15] Simser, B., Andrieux, P., Langevin, F., Parrott, T., & Turcotte, P. (2006). Field behaviour and failure modes of modified conebolts at the Craig, LaRonde and Brunswick Mines in Canada. *Deep and high stress mining*, *2*(3), 59-64.

[16] He, M., Gong, W., Wang, J., Qi, P., Tao, Z., Du, S., & Peng, Y. (2014). Development of a novel energy-absorbing bolt with extraordinarily large elongation and constant resistance. *International journal of rock mechanics and mining sciences*, *67*, 29–42. https://doi.org/10.1016/j.ijrmms.2014.01.007

[17] Varden, R., Lachenicht, R., Player, J., Thompson, A., & Villaescusa, E. (2008). Development and implementation of the garford dynamic bolt at the kanowna belle mine. *10th underground operators' conference* (pp. 95–102). The Australian institute of mining and metallurgy launceston, australia.

[18] Darlington, B., Rataj, M., Balog, G., & Barnett, D. (2018). Development of the MDX bolt and in-situ dynamic testing at telfer Gold mine. In *Rock dynamics–experiments, theories and applications* (pp. 403–408), CRC Press.

[19] Wu, Y. K., & Oldsen, J. (2010). Development of a new yielding rock bolt-yield-lok bolt. *44th us rock mechanics symposium and 5th us-canada rock mechanics symposium* (pp. 10-197). OnePetro. https://onepetro.org/ARMAUSRMS/proceedings-abstract/ARMA10/All-ARMA10/119456

[20] Chunlin Li, C. (2010). A new energy-absorbing bolt for rock support in high stress rock masses. *International journal of rock mechanics and mining sciences*, *47*(3), 396–404. https://doi.org/10.1016/j.ijrmms.2010.01.005

[21] Knox, G & Berghorst, A. (2019). Dynamic testing: determining the residual dynamic capacity of an axially strained tendon, In *Ground support 2019: proceedings of the ninth international symposium on ground support in mining and underground construction* (pp. 231-242). Australian Centre for Geomechanics. https://doi.org/10.36487/ACG_rep/1925_14_Knox

[22] Manchao, H., Leal e Sousa, R., Müller, A., Vargas, E., Ribeiro e Sousa, L., & Xin, C. (2015). Analysis of excessive deformations in tunnels for safety evaluation. *Tunnelling and underground space technology*, *45*, 190–202. https://doi.org/10.1016/j.tust.2014.09.006

[23] Wu, Z., Wu, S., & Cheng, Z. (2020). Discussion and application of a risk assessment method for spalling damage in a deep hard-rock tunnel. *Computers and geotechnics*, *124*, 103632. https://doi.org/10.1016/j.compgeo.2020.103632

[24] Li, C. C. (2021). Principles and methods of rock support for rockburst control. *Journal of rock mechanics and geotechnical engineering*, *13*(1), 46–59. https://doi.org/10.1016/j.jrmge.2020.11.001

[25] Miao, S. J., Cai, M. F., Guo, Q. F., & Huang, Z. J. (2016). Rock burst prediction based on in-situ stress and energy accumulation theory. *International journal of rock mechanics and mining sciences*, *83*, 86–94. https://doi.org/10.1016/j.ijrmms.2016.01.001

[26] Li, P., Cai, M., Guo, Q., & Miao, S. (2019). In situ stress state of the northwest region of the jiaodong peninsula, china from overcoring stress measurements in three gold mines. *Rock mechanics and rock engineering*, *52*(11), 4497–4507. DOI:10.1007/s00603-019-01827-3

[27] Feng, F., Li, X., Rostami, J., & Li, D. (2019). Modeling hard rock failure induced by structural planes around deep circular tunnels. *Engineering fracture mechanics*, *205*, 152–174. https://doi.org/10.1016/j.engfracmech.2018.10.010

[28] Wei, C., Zhang, C., Canbulat, I., & Huang, W. (2021). Numerical investigation into impacts of major fault on coal burst in longwall mining – a case study. *International journal of rock mechanics and mining sciences*, *147*, 104907. https://doi.org/10.1016/j.ijrmms.2021.104907

[29] Feng, F., Li, X., Rostami, J., Peng, D., Li, D., & Du, K. (2019). Numerical investigation of hard rock strength and fracturing under polyaxial compression based on Mogi-Coulomb failure criterion. *International journal of geomechanics*, *19*(4), 4019005.

[30] Xiao, P., Li, D., Zhao, G., & Liu, H. (2021). New criterion for the spalling failure of deep rock engineering based on energy release. *International journal of rock mechanics and mining sciences*, *148*, 104943. https://doi.org/10.1016/j.ijrmms.2021.104943

[31] Gong, F., Yan, J., Li, X., & Luo, S. (2019). A peak-strength strain energy storage index for rock burst proneness of rock materials. *International journal of rock mechanics and mining sciences*, *117*, 76–89. https://doi.org/10.1016/j.ijrmms.2019.03.020

[32] Jiang, Q., Feng, X.-T., Xiang, T.-B., & Su, G.-S. (2010). Rockburst characteristics and numerical simulation based on a new energy index: a case study of a tunnel at 2,500 m depth. *Bulletin of engineering geology and the environment*, *69*(3), 381–388. DOI:10.1007/s10064-010-0275-1

[33] Xiao, P., Li, D., Zhao, G., Zhu, Q., Liu, H., & Zhang, C. (2020). Mechanical properties and failure behavior of rock with different flaw inclinations under coupled static and dynamic loads. *Journal of central south university*, *27*(10), 2945–2958. DOI:10.1007/s11771-020-4520-x

[34] Qiu, J., Li, X., Li, D., Zhao, Y., Hu, C., & Liang, L. (2021). Physical model test on the deformation behavior of an underground tunnel under blasting disturbance. *Rock mechanics and rock engineering*, *54*(1), 91–108. DOI:10.1007/s00603-020-02249-2

[35] Zhou, Z., Cai, X., Li, X., Cao, W., & Du, X. (2020). Dynamic response and energy evolution of sandstone under coupled static–dynamic compression: insights from experimental study into deep rock engineering applications. *Rock mechanics and rock engineering*, *53*(3), 1305–1331. DOI:10.1007/s00603-019-01980-9

[36] Han, Z., Li, D., Zhou, T., Zhu, Q., & Ranjith, P. G. (2020). Experimental study of stress wave propagation and energy characteristics across rock specimens containing cemented mortar joint with various thicknesses. *International journal of rock mechanics and mining sciences*, *131*, 104352. https://doi.org/10.1016/j.ijrmms.2020.104352

[37] Qiu, S., Feng, X., Zhang, C., & Xiang, T. (2014). Estimation of rockburst wall-rock velocity invoked by slab flexure sources in deep tunnels. *Canadian geotechnical journal*, *51*(5), 520–539.

[38] He, B. G., Zelig, R., Hatzor, Y. H., & Feng, X. T. (2016). Rockburst generation in discontinuous rock masses. *Rock mechanics and rock engineering*, *49*(10), 4103–4124. DOI:10.1007/s00603-015-0906-8

[39] Skrzypkowski, K. (2020). Case studies of rock bolt support loads and rock mass monitoring for the room and pillar method in the Legnica-Głogów copper district in poland. *Energies*, *13*(11), 2998. https://www.mdpi.com/1996-1073/13/11/2998

[40] Jiang, J., Su, G., Zhang, X., & Feng, X.-T. (2020). Effect of initial damage on remotely triggered rockburst in granite: an experimental study. *Bulletin of engineering geology and the environment*, *79*(6), 3175–3194. DOI:10.1007/s10064-020-01760-8

[41] Rui, Y., Zhou, Z., Lu, J., Ullah, B., & Cai, X. (2022). A novel AE source localization method using clustering detection to eliminate abnormal arrivals. *International journal of mining science and technology*, *32*(1), 51–62. https://doi.org/10.1016/j.ijmst.2021.11.004

[42] Read, R. S. (2004). 20 years of excavation response studies at AECL's underground research laboratory. *International journal of rock mechanics and mining sciences*, *41*(8), 1251–1275. https://doi.org/10.1016/j.ijrmms.2004.09.012

[43] Kang, S. S., Ishiguro, Y., & Obara, Y. (2006). Evaluation of core disking rock stress and tensile strength via the compact conical-ended borehole overcoring technique. *International journal of rock mechanics and mining sciences*, *43*(8), 1226–1240. https://doi.org/10.1016/j.ijrmms.2006.04.007

[44] Hu, X., Su, G., Chen, G., Mei, S., Feng, X., Mei, G., & Huang, X. (2019). Experiment on rockburst process of borehole and its acoustic emission characteristics. *Rock mechanics and rock engineering*, *52*(3), 783–802. DOI:10.1007/s00603-018-1613-z

[45] Gong, F., Wuxing, W., Tianbin, L., & Xuefeng, S. (2019). Experimental simulation and investigation of spalling failure of rectangular tunnel under different three-dimensional stress states. *International journal of rock mechanics and mining sciences*, *122*, 104081. https://doi.org/10.1016/j.ijrmms.2019.104081

[46] Qiu, P., Ning, J., Wang, J., Hu, S., & Li, Z. (2021). Mitigating rock burst hazard in deep coal mines insight from dredging concentrated stress: a case study. *Tunnelling and underground space technology*, *115*, 104060. https://doi.org/10.1016/j.tust.2021.104060

[47] Tao, M., Li, X., & Li, D. (2013). Rock failure induced by dynamic unloading under 3D stress state. *Theoretical and applied fracture mechanics*, *65*, 47–54. https://doi.org/10.1016/j.tafmec.2013.05.007

[48] Feng, F., Li, X., Luo, L., Zhao, X., Chen, S., Jiang, N., … & Wang, Y. (2021). Rockburst response in hard rock owing to excavation unloading of twin tunnels at great depth. *Bulletin of engineering geology and the environment*, *80*(10), 7613–7631. DOI:10.1007/s10064-021-02377-1

[49] Ren, F., Chang, Y., & He, M. (2020). A systematic analysis method for rock failure mechanism under stress unloading conditions: a case of rock burst. *Environmental earth sciences*, *79*(15), 370. DOI:10.1007/s12665-020-09111-2

[50] Huang, R. Q., Wang, X. N., & Chan, L. S. (2001). Triaxial unloading test of rocks and its implication for rock burst. *Bulletin of engineering geology and the environment*, *60*(1), 37–41. DOI:10.1007/s100640000082

[51] Su, G., Hu, L., Feng, X., Wang, J., & Zhang, X. (2016). True triaxial experimental study of rockburst process under low frequency cyclic disturbance load combined with static load. *Rock mechanics engineer*, *35*, 1309–1322.

[52] Tarasov, B., & Potvin, Y. (2013). Universal criteria for rock brittleness estimation under triaxial compression. *International journal of rock mechanics and mining sciences*, *59*, 57–69. https://doi.org/10.1016/j.ijrmms.2012.12.011

[53] Bésuelle, P., Desrues, J., & Raynaud, S. (2000). Experimental characterisation of the localisation phenomenon inside a Vosges sandstone in a triaxial cell. *International journal of rock mechanics and mining sciences*, *37*(8), 1223–1237. https://doi.org/10.1016/S1365-1609(00)00057-5

[54] Wawersik, W. R., & Fairhurst, C. (1970). A study of brittle rock fracture in laboratory compression experiments. *International journal of rock mechanics and mining sciences & geomechanics abstracts*, *7*(5), 561–575. https://doi.org/10.1016/0148-9062(70)90007-0

[55] Kumari, W. G. P., Ranjith, P. G., Perera, M. S. A., Shao, S., Chen, B. K., Lashin, A., … & Rathnaweera, T. D. (2017). Mechanical behaviour of Australian Strathbogie granite under in-situ stress and temperature conditions: an application to geothermal energy extraction. *Geothermics*, *65*, 44–59. https://doi.org/10.1016/j.geothermics.2016.07.002

[56] Gautam, P. K., Verma, A. K., Jha, M. K., Sharma, P., & Singh, T. N. (2018). Effect of high temperature on physical and mechanical properties of Jalore granite. *Journal of applied geophysics*, *159*, 460–474. https://doi.org/10.1016/j.jappgeo.2018.07.018

[57] Li, T. B., Pan, H. S., Chen, G. Q., & Meng, L. B. (2018). Physical model tests on thermomechanical effects in rockbursts around tunnels. *Rock mechanics engineer*, *37*(2), 261-273.

[58] Yan, J., He, C., Wang, B., & Meng, W. (2019). Influence of high geotemperature on rockburst occurrence in tunnel. *Rock soil mech*, *40*(4), 1543–1550.

[59] Akdag, S., Karakus, M., Taheri, A., Nguyen, G., & Manchao, H. (2018). Effects of thermal damage on strain burst mechanism for brittle rocks under true-triaxial loading conditions. *Rock mechanics and rock engineering*, *51*(6), 1657–1682. DOI:10.1007/s00603-018-1415-3

[60] Su, G., Chen, Z., Ju, J. W., & Jiang, J. (2017). Influence of temperature on the strainburst characteristics of granite under true triaxial loading conditions. *Engineering geology*, *222*, 38–52. https://doi.org/10.1016/j.enggeo.2017.03.021

[61] He, M., Xia, H., Jia, X., Gong, W., Zhao, F., & Liang, K. (2012). Studies on classification, criteria and control of rockbursts. *Journal of rock mechanics and geotechnical engineering*, *4*(2), 97–114. https://doi.org/10.3724/SP.J.1235.2012.00097

[62] Li, S., Feng, X. T., Li, Z., Chen, B., Zhang, C., & Zhou, H. (2012). In situ monitoring of rockburst nucleation and evolution in the deeply buried tunnels of Jinping II hydropower station. *Engineering geology*, *137–138*, 85–96. https://doi.org/10.1016/j.enggeo.2012.03.010

[63] Li, X., Gong, F., Tao, M., Dong, L., Du, K., Ma, C., … & Yin, T. (2017). Failure mechanism and coupled static-dynamic loading theory in deep hard rock mining: A review. *Journal of rock mechanics and geotechnical engineering*, *9*(4), 767–782. https://doi.org/10.1016/j.jrmge.2017.04.004

[64] Kaiser, P. K., & Cai, M. (2012). Design of rock support system under rockburst condition. *Journal of rock mechanics and geotechnical engineering*, *4*(3), 215–227. https://doi.org/10.3724/SP.J.1235.2012.00215

[65] Kidybiński, A. (1981). Bursting liability indices of coal. *International journal of rock mechanics and mining sciences & geomechanics abstracts*, *18*(4), 295–304. https://doi.org/10.1016/0148-9062(81)91194-3

[66] Gong, F., Luo, S., & Yan, J. (2018). Energy storage and dissipation evolution process and characteristics of marble in three tension-type failure tests. *Rock mechanics and rock engineering*, *51*(11), 3613–3624. DOI:10.1007/s00603-018-1564-4

[67] Wang, J. A., & Park, H. D. (2001). Comprehensive prediction of rockburst based on analysis of strain energy in rocks. *Tunnelling and underground space technology*, *16*(1), 49–57. https://doi.org/10.1016/S0886-7798(01)00030-X

[68] Xu, L., Gong, F., & Luo, S. (2021). Effects of pre-existing single crack angle on mechanical behaviors and energy storage characteristics of red sandstone under uniaxial compression. *Theoretical and applied fracture mechanics*, *113*, 102933. https://doi.org/10.1016/j.tafmec.2021.102933

[69] Leveille, P., Sepehri, M., & Apel, D. B. (2017). Rockbursting potential of kimberlite: a case study of diavik diamond mine. *Rock mechanics and rock engineering*, *50*(12), 3223–3231. DOI:10.1007/s00603-017-1294-z

[70] Chen, G., Li, T., Zhang, G., Yin, H., & Zhang, H. (2014). Temperature effect of rock burst for hard rock in deep-buried tunnel. *Natural hazards*, *72*(2), 915–926. DOI:10.1007/s11069-014-1042-6

[71] Sepehri, M., Apel, D. B., Adeeb, S., Leveille, P., & Hall, R. A. (2020). Evaluation of mining-induced energy and rockburst prediction at a diamond mine in Canada using a full 3D elastoplastic finite element model. *Engineering geology*, *266*, 105457. https://doi.org/10.1016/j.enggeo.2019.105457

[72] He, Z., Gong, F., Wu, W., & Wang, W. (2021). Experimental investigation of the mechanical behaviors and energy evolution characteristics of red sandstone specimens with holes under uniaxial compression. *Bulletin of engineering geology and the environment*, *80*(7), 5845–5865. DOI:10.1007/s10064-021-02260-z

[73] Cook, N. G. W. (1976). Seismicity associated with mining. *Engineering geology*, *10*(2), 99–122. https://doi.org/10.1016/0013-7952(76)90015-6

[74] Srinivasan, C., Arora, S. K., & Yaji, R. K. (1997). Use of mining and seismological parameters as premonitors of rockbursts. *International journal of rock mechanics and mining sciences*, *34*(6), 1001–1008. https://doi.org/10.1016/S1365-1609(97)80009-3

[75] Grodner, M. (2001). Delineation of rockburst fractures with ground penetrating radar in the Witwatersrand Basin, South Africa. *International journal of rock mechanics and mining sciences*, *38*(6), 885–891. https://doi.org/10.1016/S1365-1609(01)00054-5

[76] He, M., e Sousa, L. R., Miranda, T., & Zhu, G. (2015). Rockburst laboratory tests database — application of data mining techniques. *Engineering geology*, *185*, 116–130. https://doi.org/10.1016/j.enggeo.2014.12.008

[77] Malan, D. F., & Napier, J. A. L. (2018). Rockburst support in shallow-dipping tabular stopes at great depth. *International journal of rock mechanics and mining sciences*, *112*, 302–312. https://doi.org/10.1016/j.ijrmms.2018.10.026

[78] Ortlepp, W. D., & Stacey, T. R. (1994). Rockburst mechanisms in tunnels and shafts. *Tunnelling and underground space technology*, *9*(1), 59–65. https://doi.org/10.1016/0886-7798(94)90010-8

[79] Cai, M. (2016). Prediction and prevention of rockburst in metal mines – A case study of Sanshandao gold mine. *Journal of rock mechanics and geotechnical engineering*, *8*(2), 204–211. https://doi.org/10.1016/j.jrmge.2015.11.002

[80] Meng, F., Zhou, H., Wang, Z., Zhang, L., Kong, L., Li, S., & Zhang, C. (2016). Experimental study on the prediction of rockburst hazards induced by dynamic structural plane shearing in deeply buried hard rock tunnels. *International journal of rock mechanics and mining sciences*, *86*, 210–223. https://doi.org/10.1016/j.ijrmms.2016.04.013

[81] Keneti, A., & Sainsbury, B. A. (2018). Review of published rockburst events and their contributing factors. *Engineering geology*, *246*, 361–373. https://doi.org/10.1016/j.enggeo.2018.10.005

[82] Singh, S. P. (1989). Classification of mine workings according to their rockburst proneness. *Mining science and technology*, *8*(3), 253–262. https://doi.org/10.1016/S0167-9031(89)90404-0

[83] Tang, L. Z., Pan, C. L., & Wang, W. (2002). Surplus energy index for analysing rock burst proneness. *Journal of central south university of technology (China)*, *33*(2), 129-132.

[84] Singh, S. P. (1988). Burst energy release index. *Rock mechanics and rock engineering*, *21*(2), 149–155. DOI:10.1007/BF01043119

[85] Zhang, C. Q., Lu, J. J., Chen, J., Zhou, H., & Yang, F. J. (2017). Discussion on rock burst proneness indexes and their relation. *Rock and soil mechanics, 38*(5), 1397-1404. DOI:10.16285/j.rsm.2017.05.022

[86] Xiao, P., Li, D., & Zhu, Q. (2022). Strain energy release and deep rock failure due to excavation in pre-stressed rock. *Minerals, 12*(4), 488.

[87] Tang, L., Yang, C., & Pan, C. (2006). Optimization of microseismic monitoring network for large-scale deep well mining. *Chinese journal of rock mechanics and engineering, 25*(10), 2036–2042.

[88] Steinberg, D. M., & Rabinowitz, N. (2003). Optimal seismic monitoring for event location with application to on site inspection of the comprehensive nuclear test ban treaty. *Metrika, 58*(1), 31–57. DOI:10.1007/s001840200222

[89] Kijko, A. (1977). An algorithm for the optimum distribution of a regional seismic network—I. *Pure and applied geophysics, 115*(4), 999–1009. DOI:10.1007/BF00881222

[90] Kijko, A. (1977). An algorithm for the optimum distribution of a regional seismic network — II. an analysis of the accuracy of location of local earthquakes depending on the number of seismic stations. *Pure and applied geophysics, 115*(4), 1011–1021. DOI:10.1007/BF00881223

[91] Kaiser, P. K., Vasak, P., Suorineni, F. T., & Thibodeau, D. (2005). New dimensions in seismic data interpretation with 3-D virtual reality visualization for burst-prone mines. *RaSiM6: proceedings of the sixth international symposium on rockburst and seismicity in mines proceedings, australian centre for geomechanics, perth* (pp. 33-45). Australian centre for geomechanics. https://doi.org/10.36487/ACG_repo/574_0.3

[92] Vasak, P., Suorineni, F. T., & Verma, A. (2004). Identification of seismically active structures for hazard assessment at Creighton Mine. *Report submitted to inco mines technology department*.

[93] Zhuang, Z., Liu, Z., Cheng, B., & Liao, J. (2014). Fundamental Linear Elastic Fracture Mechanics. In *Extended finite element method, academic press, oxford* (pp. 11-52), Elsevier Science. https://doi.org/10.1093/oso/9780192846242.003.0002